[5] J. P. Webb, G. L. Maile, and R. L. Ferrari, "Finite element solution of three-dimensional electromagnetic problems," *Proc. Inst. Elec. Eng.*, vol. 130, pt. H, no. 2, pp. 153–159, Mar. 1983.
[6] M. Hara, T. Wada, T. Fukasawa, and F. Kikuchi, "Three dimensional analysis of RF electromagnetic fields by finite element method," *IEEE Trans. Magn.*, vol. MAG-19, no. 6, pp. 2417–2420, 1983.
[7] J. B. Davies, F. A. Fernandez, and G. Y. Philippou, "Finite element analysis of all modes in cavities with circular symmetry," *IEEE Trans. Microwave Theory Tech.*, vol. MTT-30, pp. 1975–1980, Nov. 1982.
[8] B. M. A. Rahman and J. B. Davies, "Finite-element analysis of optical and microwave problems," *IEEE Trans. Microwave Theory Tech.*, vol. MTT-32, pp. 20–28, Jan. 1984.
[9] Z. J. Csendes and P. Silvester, "Numerical solution of dielectric loaded waveguides: I—Finite element analysis," *IEEE Trans. Microwave Theory Tech.*, vol. MTT-18, pp. 1124–1131, Dec. 1970.
[10] A. Konrad, "Vector variational formulation of electromagnetic fields in anisotropic media," *IEEE Trans. Microwave Theory Tech.*, vol. MTT-24, pp. 553–559, 1976.
[11] A. D. Berk, "Variational principles for electromagnetic resonators and waveguides," *IRE Trans. Antennas Propagat.*, vol. AP-4, pp. 104–110, Apr. 1956.
[12] P. Silvester and R. L. Ferrari, *Finite Elements for Electrical Engineers*. Cambridge, England: Cambridge University Press, 1983.
[13] S. Ramo, J. R. Whinnery, and T. Van Duzer, *Fields and Waves in Communication Electronics*. New York: Wiley, 1965.
[14] A. H. Sameh and J. A. Wisniewski, "A trace of minimization algorithm for the generalized eigenvalue problem," *SIAM J. Numer. Anal.*, vol. 19, no. 6, pp. 1243–1259, Dec. 1982.

Large-Signal Microwave Performance Prediction of Dual-Gate GaAs MESFET Using an Efficient and Accurate Model

ASHER MADJAR, SENIOR MEMBER, IEEE,
AND JONA DREIFUSS

Abstract—**This paper presents a microwave large-signal model for the dual-gate MESFET. The model enables prediction of device performance in small-signal and large-signal circuits. The model is an extension of a previously developed model for the ordinary MESFET. It relies on basic principles, thus correlating the device geometry and physical parameters to its performance. The speed and accuracy of the model are demonstrated by calculating three types of device performances: dc curves, small-signal scattering parameters, and large-signal simulation of an amplifier. Good agreement was achieved between calculated and measured performance. The computed results are presented for comparison only, and no attempt was made to present a comprehensive analysis of the device performance.**

I. Introduction

Increasingly, dual-gate GaAs MESFET devices are finding use in microwave circuits. In recent years, many researchers have investigated the device properties and applications. The most useful applications which have emerged thus far are: AGC amplifiers, mixers (including self-oscillating) [1]–[3], active phase shifters [2], [4], frequency multipliers [2], [5], power combiners/dividers [6], and up converters [7].

Small-signal circuits can be conveniently analyzed and designed by use of measured scattering parameters. However, in most of the above applications, the device operates in a large-signal mode. Large-signal circuits can be built, of course, experimentally, but this involves much "cut and try" effort. The best approach to nonlinear circuit development is to design the circuit theoretically (approximate design is usually acceptable), build it, and fine-tune it to the desired performance. This latter approach requires an efficient and reasonably accurate model for the device.

This paper presents such a model for the dual-gate MESFET. Its speed and accuracy are demonstrated by calculating the device performance and comparing it to the measured performance presented in the manufacturer's data sheet.

Manuscript received February 21, 1984; revised February 11, 1985.
The authors are with RAFAEL, Electronics Division, P.O. Box 2250, 31021 Haifa, Israel.

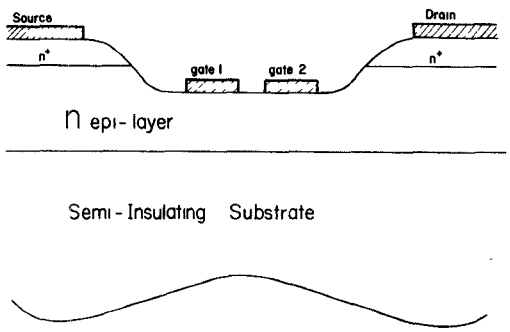

Fig. 1. Dual-gate MESFET cross-section view.

II. Device Structure

The physical structure of the device is presented in Fig. 1. As shown, the structure is similar to an ordinary FET except for the two gates. The device is built on a semi-insulating substrate of GaAs. An n-type epitaxial active layer is grown on the substrate, and on top of it an n^+ layer. The source and drain electrodes form ohmic contacts to the GaAs material, while the two gate electrodes form Schottky-barrier junctions.

From Fig. 1, it is obvious that this device is basically a combination of two ordinary MESFET's. In fact, Asai *et al.* [8], [9] have shown that electrically this device is a cascade connection of two ordinary FET's, the first in a common-source mode and the second in a common-gate mode. (See Fig. 3(a)).

III. The Model

An efficient and accurate microwave large-signal model for the ordinary MESFET was developed by Madjar and Rosenbaum [10]–[12]. This model was developed using basic principles, namely, solving the electric-field problem in the device in an approximate analytical fashion. This approach yielded a model which has advantages in all respects: it is fast, it related the physical device parameters to its electrical performance, and it has reasonable accuracy. The exact details of the model are presented in the above references.

The circuit diagram of an ordinary assembled FET is presented in Fig. 2. The "box" in the center of the diagram represents the active part of the device. This part is characterized by the computer model as follows:

$$I_g(t) = GVSG\frac{dV_{SG}(t)}{dt} + GVDS\frac{dV_{DS}(t)}{dt} \tag{1}$$

$$I_d(t) = I_{\text{con}} + DVSG\frac{dV_{SG}(t)}{dt} + DVDS\frac{dV_{DS}(t)}{dt}. \tag{2}$$

I_{con} and the four capacitive coefficients are functions of V_{SG}, V_{DS} and are computed by the model.

The other components in Fig. 2 are parasitic elements, which are undesirable but must be taken into account. The two diodes

0018-9480/85/0700-0639$01.00 ©1985 IEEE

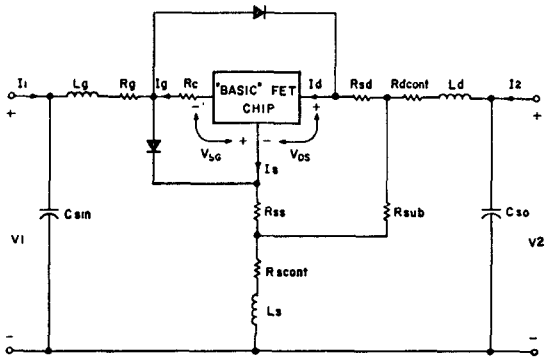

Fig. 2. Assembled MESFET circuit diagram.

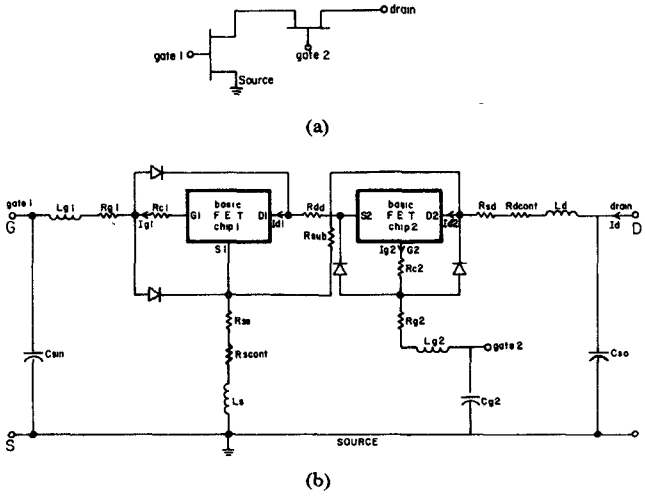

Fig. 3. Circuit diagram for dual-gate MESFET. (a) General cascade connection. (b) Detailed circuit.

represent the Schottky-barrier junctions. R_c is the "charging resistor" for the channel [10] and is computed by the model for each pair of values V_{SG} and V_{DS}. R_{ss} and R_{sd} are constant bulk resistances of the GaAs between electrodes. R_g, $R_{s\text{cont}}$, $R_{d\text{cont}}$ are contact resistances. L_g, L_s, and L_d are wire bond inductances. C_{sin}, C_{so} are parasitic capacitances. R_{sub} is substrate leakage resistance.

This previously developed model can be used effectively to simulate and predict the performance of the dual-gate device as outlined below. As discussed above, the dual-gate FET is electrically equivalent to two ordinary FET's connected in cascade. Thus, using the model of an ordinary FET (Fig. 2), the circuit model for the dual-gate device emerges as presented in Fig. 3.

Since this is a four-terminal device, there are four sets of external parasitic elements (instead of three in an ordinary FET). Also, there is an additional bulk resistance R_{dd}–intergate resistance.

The circuit in Fig. 3 completely characterizes the device by using (1) and (2) for both "boxes" and writing the circuit equations for the rest of the network.

IV. DC and Small-Signal Simulations

The dc curves of the device describe the dependence of the dc drain current on the dc terminal voltage: $V_{SG_1}, V_{SG_2}, V_{DS}$. To achieve this goal, the internal voltages across each one of the two devices in Fig. 3 must be calculated for a given set of external

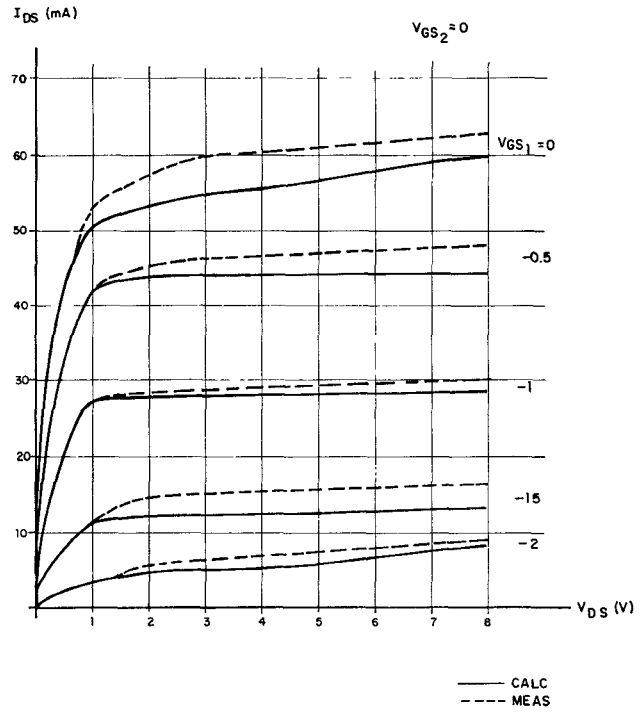

Fig. 4 DC curves for RDX832.

TABLE I
Device Parameters for RDX832

EPI layer thickness = 0.2 μm.

Doping level = 10^{17} cm^{-3}

Gates lengths = 1 μm; Gates widths = 500μm

$R_{dd} = R_{ss} = 1.56\Omega$; $R_{sd} = 3.13\Omega$

$R_{scont} = 1\Omega$; $R_{dcont} = R_g = 2\Omega$; $R_{sub} = 1000\Omega$

Lg = 0.4 nHy ; Ls = 0.1 nHy ; Ld = 0.55 nHy

$C_{sin} = C_{so} = C_{g_2} = 0.2$PF

bias voltages. The dc equations of the circuit are

$$V_{S_1G_1} - V_{SG_1} - R_s \cdot I_d = 0 \quad (3)$$

$$V_{D_1S_1} - V_{S_2G_2} + V_{SG_2} + (R_{dd} + R_s) \cdot I_d = 0 \quad (4)$$

$$V_{D_1S_1} + V_{D_2S_2} - V_{DS} + (R_s + R_d + R_{dd}) I_d = 0 \quad (5)$$

$$V_{D_1S_1} - V_{D_2S_2} \cdot R_{\text{sub}_1}/R_{\text{sub}_2} + R_{\text{sub}_1}(I_{d_1} - I_{d_2}) = 0 \quad (6)$$

where

$$R_s = R_{ss} + R_{s\text{cont}} \quad R_d = R_{sd} + R_{d\text{cont}} \quad I_d = I_{d_2} + V_{D_2S_2}/R_{\text{sub}_2}.$$

This set of nonlinear equations is solved using the subroutine ZSPOW from the IMSL package (the nonlinearity is due to I_{d_1}, I_{d_2}, which are calculated using (2)). The calculated versus measured dc curves of the Raytheon RDX832 device are presented in Fig. 4. The device parameters used in the simulation are presented in Table I.

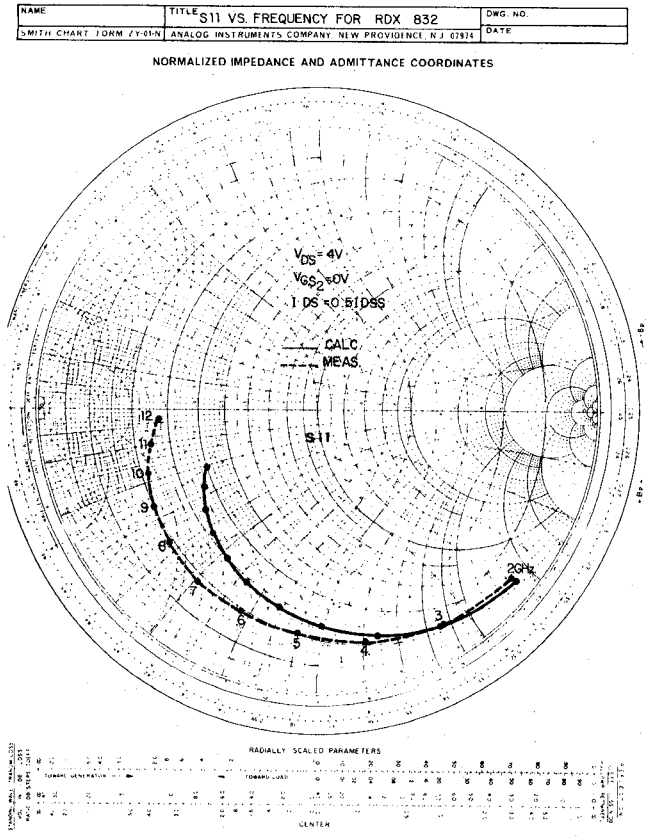

(a)

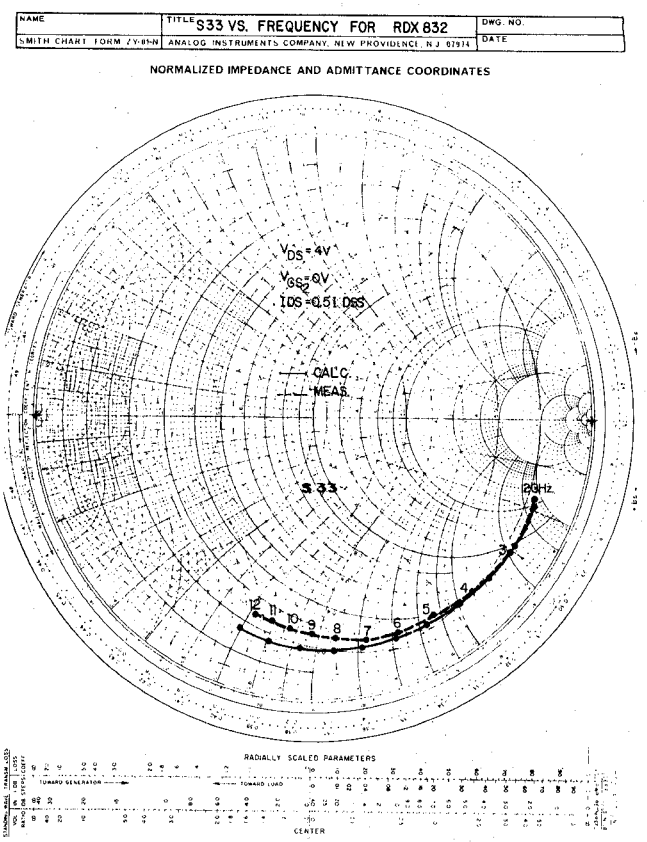

(b)

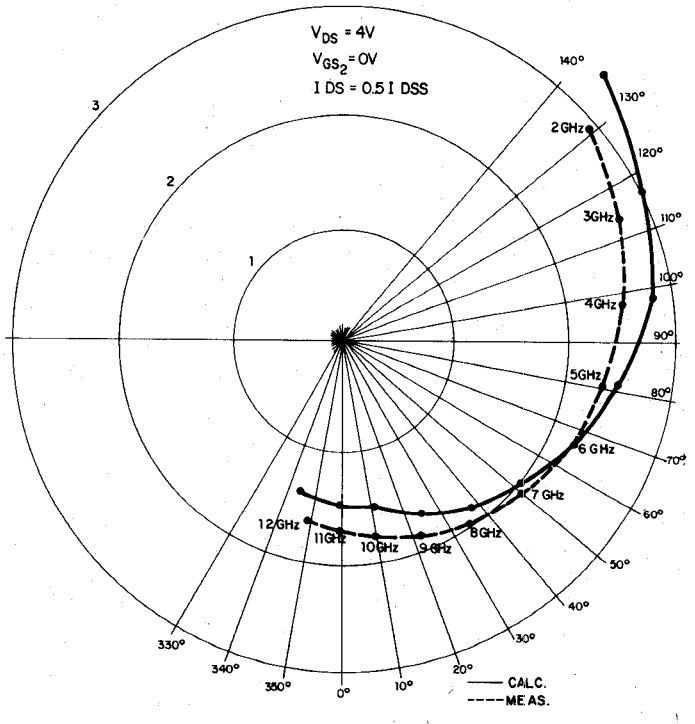

(c)

Fig. 5. Small-signal scattering parameters for RDX832. (a) S_{11}. (b) S_{33}. (c) S_{31}.

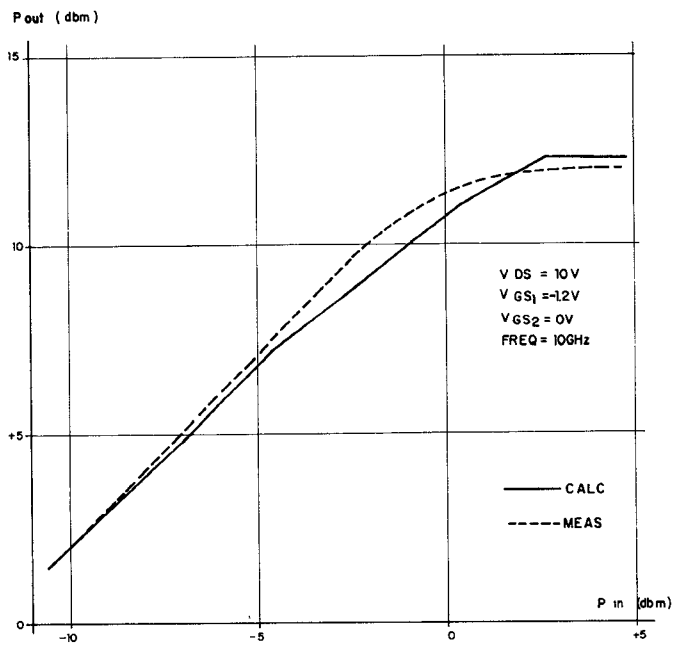

Fig. 6 Saturation curve for RDX832.

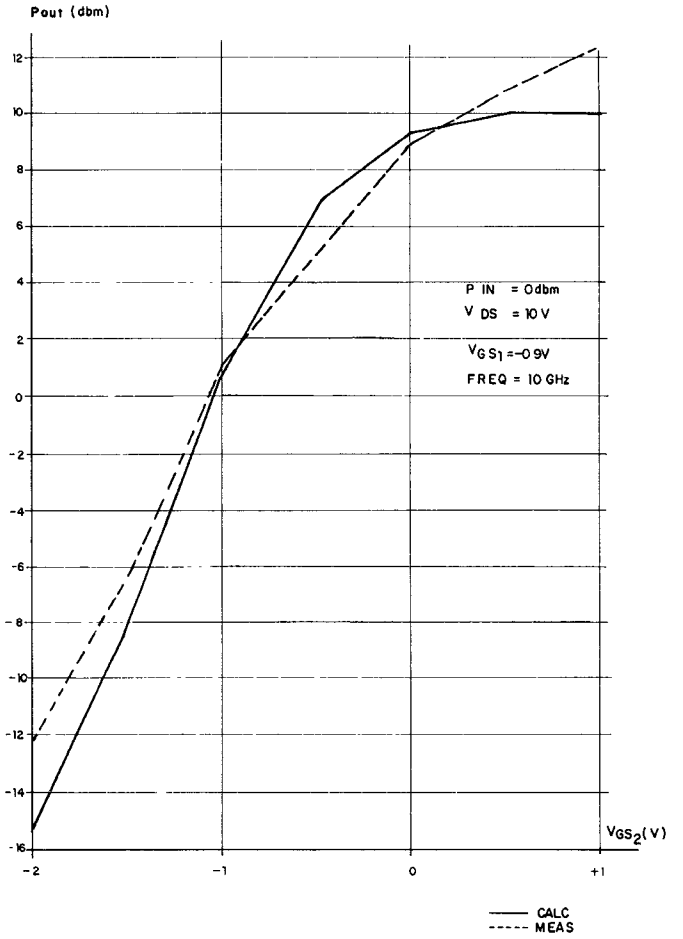

Fig. 7 *AGC* characteristic of RDX832.

The small-signal scattering parameters for a given bias point are calculated by the following procedure:

1) Calculate the *s*-parameters of each "partial FET" in the ordinary way as outlined in [10].
2) Convert the *s*-parameters into *ABCD* parameters using the standard conversion formulas.
3) Multiply the two *ABCD* matrices to get the *ABCD* matrix of the device.
4) Convert the *ABCD* parameters into *s*-parameters.

The computed scattering parameters of the RDX832 device are presented in Fig. 5, along with the measured data from the manufacturer's data sheet (port 1 ≡ gate 1, port 2 ≡ gate 2, port 3 ≡ drain). The measured versus computed comparison is given for the gate 1 − drain parameters, since only these are presented in the data sheet.

The parameter S_{13} is very small and comparable in magnitude to the value given in the data sheet. The other five parameters ($S_{22}, S_{32}, S_{23}, S_{21}, S_{12}$) were computed by us; however, since this data is not supplied by the manufacturer, no comparison was made. It is worth noting that S_{22} is very close to S_{33}.

V. Large-Signal Simulations

To demonstrate the capability and efficiency of the model, a large-signal simulation was performed using the RDX832. The simulated circuit is a simple amplifier including the device itself (Fig. 3), a 10-GHz signal generator connected between source and gate 1 (including its impedance), and a load impedance connected between drain and source. The generator and load impedances were chosen for maximum small-signal gain.

The simulation was performed by the harmonic balance method, which is very efficient and allows fast calculation of the steady-state solution. The simulation follows the general approach outlined in [13], except that the resulting set of nonlinear equations was solved by the subroutine ZSPOW as above.

Using this computer program simulation, two curves were computed and presented along with the measured data from the manufacturer's data sheet.

1) Saturation curve of the amplifier (Fig. 6). This curve displays the output power versus input power up to the beginning of power saturation taking into account four harmonics. Short circuit was used for the second-gate load for all harmonics.

2) *AGC* curve (Fig. 7). This curve displays the output power versus the second-gate dc voltage with the input power held constant at 0 dBm taking into account 15 harmonics. A 50-Ω load was used at the second gate for all harmonics.

The generation of these curves was performed by running the program repeatedly for several input power values (Fig. 6) or second-gate voltage values (Fig. 7). A typical run of the program takes approximately 10 to 15 s of CPU time on CDC6600.

VI. Conclusion

A microwave large-signal model for the dual-gate FET was introduced. The model is very fast, reasonably accurate, and directly relates the electrical performance to the physical parameters. The usefulness of the model was demonstrated by comparing simulation results to measured performance.

References

[1] C. Tsironis, "12 GHz receiver with a self-oscillating dual gate MESFET mixer," *ACTA Electronica*, vol. 23, no. 4, pp. 325–329, 1980.
[2] C. Tsironis, "GaAs dual MESFETs and their applications in microwave circuits," *ACTA Electronica*, vol. 23, no. 4, pp. 317–324, 1980.
[3] C. Tsironis *et al.*, "Modelling and evaluation of dual gate MESFETs as low noise self-oscillating and image rejection mixers," in *1983 IEEE MTT-S Dig.*
[4] S. P. Mazumder *et al.*, "A frequency translator using dual gate GaAs FETs," in *1983 IEEE MTT-S Dig.*
[5] R. Stancliff, "Balanced dual gate GaAs FET frequency doublers," in *1981 IEEE MTT-S Dig.*
[6] J. J. Pan, "Active microwave power combiner/divider using a dual gate MESFET," in *1981 IEEE MTT-S Dig.*

[7] A. A. de Salles, "Design and performance of dual gate GaAs MESFET up converter," in *1983 IEEE MTT-S Dig.*
[8] S. Asai *et al.*, "The GaAs dual-gate FET with low noise and wide dynamic range," in *IEEE Int. Electron Devices Meet. Dig.*, 1973, pp. 64-67.
[9] S. Asai *et al.*, "GaAs dual-gate Schottky-barrier FET's for microwave frequencies," *IEEE Trans. Electron Devices*, vol. ED-22, pp. 897-904, Oct. 1975.
[10] A. Madjar and F. J. Rosenbaum, "An ac large signal model for the GaAs MESFET," Dept. Elec. Eng., Washington University, St. Louis, MO, Final Rep. Contract N00014-78-C-0256, Aug. 1979.
[11] A. Madjar and F. J. Rosenbaum, "A practical ac large signal model for GaAs microwave MESFET," in *1979 IEEE MTT-S Dig.*
[12] A. Madjar and F. J. Rosenbaum, "A large signal model for the GaAs MESFET," IEEE *Trans. Microwave Theory Tech.*, vol. MTT-29, pp. 781-788, Aug. 1981.
[13] D. R. Green, Jr. and F. J. Rosenbaum, "Performance limits on GaAs FET large and small signal circuits," Dept. Elec. Eng., Washington University, St. Louis, MO, Rep. NRL-81-1 Contract N00014-80-0318, Oct. 1981.

Analysis of Asymmetric Coupled Striplines

TOSHIHIDE KITAZAWA AND RAJ MITTRA, FELLOW, IEEE

***Abstract*—A unified method for the quasi-static and the hybrid-mode formulation of asymmetric coupled striplines is presented. Variational expressions are derived for the matrix elements, which describe the quasi-static characteristics, for the first time. A very accurate numerical method is shown and some numerical examples are presented for the different types of asymmetric coupled striplines with anisotropic substrates.**

I. Introduction

Asymmetric coupled striplines have received considerable attention in recent years [1]–[7]. When these lines are used as building blocks for filters and directional couplers, they can provide additional advantages compared with the symmetric cases because of their impedance transform nature and flexibility.

Although accurate analytical methods of symmetrical cases are available for different types of coupled striplines [8], [9] based on the quasi-static and hybrid-mode formulations, fewer techniques have been reported for only coupled microstrips on isotropic substrates [1], [3]. Most of them are the quasi-static case; however, the variational expression for the quasi-static parameters have not been derived. In this paper, a unified analytical method is presented for the asymmetric coupled striplines. It gives the variational expressions for the matrix elements which describe the quasi-static characteristics and also it gives the hybrid-mode analysis for the frequency-dependent solutions. The formulation is general enough to treat coupled microstrips, strips with overlay, and suspended strips on anisotropic substrates. Some numerical examples are presented for the quasi-static and frequency-dependent cases.

II. Analytical Method

Fig. 1 shows the general structure of asymmetric coupled striplines with multilayered uniaxially anisotropic media, whose permittivity dyadics are

$$\bar{\bar{\epsilon}}_i = \epsilon_0(\epsilon_{i\perp}\hat{x}_0\hat{x}_0 + \epsilon_{i\perp}\hat{y}_0\hat{y}_0 + \epsilon_{i\parallel}\hat{z}_0\hat{z}_0). \quad (1)$$

Manuscript received October 1, 1984; revised February 25, 1985.

T. Kitazawa is with the Department of Electrical Engineering, Kitami Institute of Technology, Kitami 090, Japan.
R. Mittra is with the Department of Electronic Engineering, University of Illinois, Urbana, IL 61801.

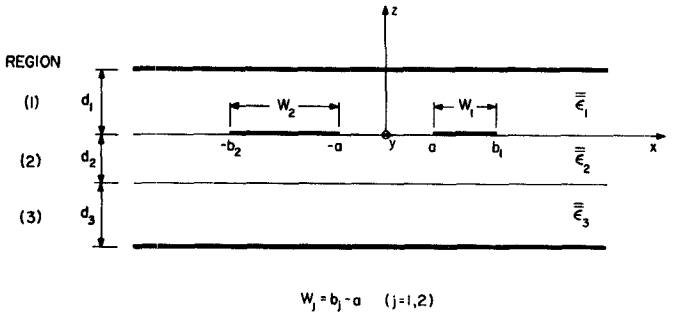

Fig. 1. General structure of the asymmetric coupled striplines.

The electric fields in each region can be expressed in terms of current density on the strips $\hat{i}(x')$ by using the extended version of the method in [9]

$$\hat{E}^{(i)}(x,y,z) = -\int_{x'}\int_{z'} \bar{\bar{Z}}^{(i)}(x,z|x',z')\cdot\hat{i}(x')\delta(z')\,dz'\,dx' \cdot e^{-j\beta_0 y}\cdot(i=1,2,3) \quad (2)$$

where β_0 is the propagation constant in the y-direction and the dyadic Green's function $\bar{\bar{Z}}^{(i)}$ is given by

$$\bar{\bar{Z}}^{(i)}(x,z|x',z') = \frac{1}{2\pi}\sum_{l=1}^{2}\int_{-\infty}^{\infty}\left[\frac{\hat{K}_l}{K^2}Z_l^{(i)}(z|z') - \frac{\hat{z}_0}{\omega\epsilon_0\epsilon_{l\parallel}}\delta_{l1}T_l^{(i)}(z|z')\right]\cdot\hat{K}_l e^{j\alpha(x'-x)}\,d\alpha$$

$$\hat{K}_1 = \hat{x}_0\alpha + \hat{y}_0\beta_0$$

$$\hat{K}_2 = \hat{K}_1\times\hat{z}_0$$

$$K = \sqrt{\alpha^2+\beta_0^2}. \quad (3)$$

The scalar Green's function $Z_l^{(i)}, T_l^{(i)}$ in (3) can be derived by applying the conventional circuit theory to the equivalent circuits shown in Fig. 2 [9]. The field representation (2) is exact and it gives the basis for both the quasi-static and the hybrid-mode formulations.

A. Variational Expressions for the Quasi-Static Parameters

The capacitance matrix has been used to describe the quasi-static characteristics of asymmetric coupled lines [1], [2] and it is defined as

$$\begin{bmatrix} Q_1 \\ Q_2 \end{bmatrix} = \begin{bmatrix} C_1 & -C_m \\ -C_m & C_2 \end{bmatrix}\begin{bmatrix} V_1 \\ V_2 \end{bmatrix} \quad (4)$$

where V_1 and Q_1 are the potential and the total charges on the right strip ($a < x < b_1$), and V_2 and Q_2 are those on the left strip ($-b_2 < x < -a$), and C_1, C_2, and C_m are the self and mutual capacitances. However, to the authors' knowledge, the variational expressions for these matrix elements have not been derived even for the coupled microstrips with the isotropic substrate. In what follows, the compliance matrix, the inverse matrix of the capacitance matrix, is introduced to describe the quasi-static characteristics of the asymmetric coupled striplines, and the variational expressions for the matrix elements are derived for the general structure shown in Fig. 1.

0018-9480/85/0700-0643$01.00 ©1985 IEEE